



The effect of titanium dioxide nano-filler on the conductivity, morphology and thermal stability of poly(methyl methacrylate)—poly(styrene-co-acrylonitrile) based composite solid polymer electrolytes

S. V. Ganesan¹ · K. K. Mothilal¹ · S. Selvasekarapandian² · T. K. Ganesan³

Received: 7 August 2017 / Accepted: 23 February 2018 / Published online: 26 February 2018
© Springer Science+Business Media, LLC, part of Springer Nature 2018

Abstract

The composite solid polymer electrolyte (CSPE) samples, comprising of poly(methylmethacrylate) (PMMA)/poly(styrene-co-acrylonitrile) (SAN)/ethylene carbonate (EC)/propylene carbonate (PC)/lithium trifluoromethanesulfonate (LiCF₃SO₃)/anatase-TiO₂ as nano-filler (0, 5, 6, 7, 8 and 9 wt% for samples T0, T1, T2, T3, T4 and T5 respectively) were prepared by solution casting technique. Fourier transform infrared (FT-IR) spectral studies indicate the interaction of PMMA and plasticizers (EC, PC) with Lithium ion and nano-filler TiO₂ in samples. From AC impedance studies ionic conductivity, dielectric constant increase with increase in the concentration of nano-filler TiO₂ up to 9 wt%. The sample T5 shows lowest activation energy (E_a) of 0.14 eV, very short relaxation time (τ) of 1.49×10^{-7} s and exhibits maximum ionic conductivity of 1.05×10^{-4} S cm⁻¹ at room temperature. The conductivity-temperature dependence studies showed that the conductivity of all samples depict Arrhenius behaviour suggesting ion-hopping mechanism. Dielectric studies reveal ion conducting nature of CSPE samples. Thermogravimetric analysis indicate the thermal stability of CSPE sample T5 up to 333 °C with maximum degradation at 388 °C. DSC studies reveal absence of glass transition temperature (T_g) of atactic component of PMMA in CSPE sample T5 indicating amorphous nature. X-ray diffraction patterns shows shift in the position of peaks confirming the complex formation of the PMMA-SAN-EC-PC-LiCF₃SO₃-TiO₂ system. SEM analysis indicates that the presence of lithium salt and filler TiO₂ on polymer host does not lead to heterogenous polymer blend thus retaining its amorphous nature.

1 Introduction

Recently, there is increasing demand worldwide for a sustainable, safe, clean and environment friendly energy resources. Polymer electrolytes, particularly, involving lithium ion batteries play a key role in meeting the above demands of modern energy technology. In order to enhance the conductivity and stability of polymer electrolytes,

combination of several approaches like co-polymerisation, blending and addition of plasticizers lead to solvent free solid polymer electrolytes (SPE). Addition of plasticizers with high dielectric constant (ϵ) such as propylene carbonate ($\epsilon = 64.4$) and ethylene carbonate ($\epsilon = 89.6$) improve the amorphous nature of the polymer electrolyte and enhance its ionic conductivity [1, 2]. In plasticized polymer electrolytes, the salt-solvating power and sufficient ionic mobility is provided by the plasticizer [3]. Another approach is dispersing inorganic inert ceramic fillers such as SiO₂, Al₂O₃, and TiO₂ etc., into the solid polymer electrolyte and developing the composite solid polymer electrolyte (CSPE). Ahmad et al. [4] and Adebahr et al. [5] reported that the dispersion of nano-sized ceramic fillers not only enhances mechanical strength, but also increases its ionic conductivity. Adebahr et al. claimed that dispersion of filler into the PMMA based electrolyte system decreases the polymer/cation interaction and introduces a new pathway for conduction of lithium ions. The Lewis acid-base interaction between the electrolyte

✉ S. V. Ganesan
svganesan10@gmail.com

✉ K. K. Mothilal
mothi63@yahoo.com

¹ Department of Chemistry, Saraswathi Narayanan College, Madurai, Tamil Nadu 625 022, India

² Materials Research Centre, Coimbatore, Tamil Nadu 641 001, India

³ Department of Chemistry, The American College, Madurai, Tamil Nadu 625 002, India

ionic species and polar surface groups of the inorganic solid oxide fillers lead to formation of ion-ceramic filler complex and thus greater degree of dissociation of electrolyte salt [6, 7]. Besides, the use of ceramic filler tends to decrease the glass transition temperature (T_g) and crystallinity of the polymer, and therefore allow amorphous polymer to maintain liquid-like characteristics and enhance their conductivity [8]. The mechanical strength and the electrochemical performance of the electrolytes are expected to increase with the decreasing filler size [9, 10]. Furthermore, addition of ceramic filler can also prevent polymer chain reorganisation, which promotes the ion transportation and improves the interfacial, electrochemical stability and mechanical properties of the polymer electrolyte [9].

Most research has emphasised on blending of crystalline polymer like PEO, PVdF or semi-crystalline polymer like PVdF-HFP blend with amorphous polymers like PMMA, PVC, and PVA [3] in order to reduce crystallinity and enhance ionic conductivity in amorphous phase. Therefore, in this study, the blending of two amorphous polymers, namely PMMA and SAN with lithium triflate salt and crystalline nano-filler TiO_2 is carried out in the presence of plasticizers EC and PC. G.N. Kumaraswamy et al. [11] and Miao et al. [12] have described that 10–30% of PMMA is the miscibility window for PMMA/SAN blend system. Beyond 30% though the blend system is miscible yet, the hydrodynamic parameters and phase separation temperatures seems to decrease suggesting immiscibility at higher temperatures (above 160 °C). There are several studies reported in literature involving PMMA as host polymer [13]. Solid polymer electrolytes incorporating lithium triflate and nanofillers into the PMMA host have reported enhanced conductivity [14, 15]. But the thermal stability and shelf life of such systems are too low. The polymer electrolytes involving PMMA host starts to degrade at around 160 °C. In order to enhance the thermal stability of the polymer electrolytes involving PMMA, the host PMMA is blend with SAN polymer which possesses high stability. The melting temperature of SAN is above 300 °C. The morphology, conduction and rheological behaviours of PMMA/SAN blend nanocomposites incorporating multiwallcarbon nanotubes and chemically reduced graphene oxide fillers have been studied at higher temperatures [16–19]. To our knowledge, there are no reports on the conductivity studies of polymer electrolyte involving PMMA-SAN blend with nano-fillers at ambient temperatures. Lithium ions are known to interact with nano-filler TiO_2 thus utilising it for its transport and hence enhanced ionic conductivity. The incorporation of nano-filler also enhances mechanical stability of the polymer electrolyte system [20]. The plasticizers EC and PC are known to solvate lithium ions as well as nano-fillers promoting homogeneity and enhanced interaction between polymer host, filler and lithium salt leading to enhanced ionic conductivity. Thus, in

the present study, attempt has been made to study the effect of varying concentration of nano-sized filler anatase- TiO_2 on the conductivity, morphology and thermal stability of the composite solid polymer electrolyte system comprising of PMMA, SAN, EC, PC and Lithium triflate.

2 Materials and methods

2.1 Sample preparation

All the samples were prepared by a solution casting technique [9]. The polymers poly(methylmethacrylate) (PMMA, Avg. $M_w = 5.5 \times 10^5$) and poly(styrene-*co*-acrylonitrile) (SAN, Avg. $M_w = 1.65 \times 10^5$) were purchased from Alfa-Aesar and Sigma-Aldrich respectively. SAN was dried at 100 °C in an oven for 10 h before use. The plasticizer, ethylene carbonate (EC) (99%) and propylene carbonate (PC) (99%) were purchased from Alfa-Aesar respectively and used as such. The Lithium triflate salt ($LiCF_3SO_3$) with 99.995% purity was purchased from Sigma-Aldrich and dried at 100 °C for 2 h before carrying out reactions. The inorganic nano-sized filler anatase- TiO_2 99.7% (32 nm) was purchased from Alfa-Aesar and dried in oven at 100 °C prior to use. The solvent THF (Tetrahydrofuran) with 99.9% purity was purchased from SRL and used as such.

Stoichiometric quantities of PMMA and SAN polymers were dissolved in 10 ml THF solvent and followed by mechanical stirring for 8 h to obtain uniform mixture of the blend. The $LiCF_3SO_3$ (18 wt%) salt was added to another conical flask containing stoichiometric quantities of plasticizers ethylene carbonate and propylene carbonate in 10 ml THF solvent and stirred well for few hours using mechanical stirrer until clear transparent solution is formed. The contents of the conical flask were carefully and meticulously transferred to the conical flask containing polymer blends, stirred well for few hours at room temperature. Varying concentration of nanofiller TiO_2 (5, 6, 7, 8, 9 wt%) was added to the above system and stirred for 24 h at room temperature and at 60 °C for few hours before casting the solution onto a petri dish. The solvent THF was allowed to evaporate slowly at room temperature for 24 h until then the polymer electrolyte film is formed. The traces of the solvent were removed by drying at 70 °C in a vacuum oven for ~2 days. The samples were then kept in dessicator for further drying and then used for different experimental studies. The composite solid polymer electrolyte samples were labelled T0, T1, T2, T3, T4, and T5 according to filler concentration (in wt%) of 0, 5, 6, 7, 8, and 9 respectively (Table 1).

Table 1 Composition in weight and its percentage for each of the CSPE sample prepared in 20 ml of THF solvent

#	PMMA		SAN		EC		PC		LiCF ₃ SO ₃		TiO ₂	
	g	wt%	g	wt%	g	wt%	g	wt%	g	wt%	g	wt%
T0	1.01	26.4	0.99	25.9	0.56	14.7	0.56	14.7	0.70	18.3	0.00	0.0
T1	0.99	26.0	0.98	25.8	0.49	12.9	0.45	11.9	0.70	18.4	0.19	5.0
T2	0.99	26.0	0.99	26.0	0.45	11.9	0.45	11.9	0.70	18.4	0.23	5.9
T3	1.01	26.4	0.99	25.8	0.45	11.8	0.42	10.8	0.70	18.3	0.27	6.9
T4	0.98	25.8	0.99	26.0	0.42	10.9	0.42	10.9	0.70	18.4	0.30	7.9
T5	1.01	26.3	0.98	25.6	0.42	10.8	0.39	10.2	0.70	18.3	0.34	8.9

2.2 Measurements

The X-Ray Diffraction (XRD) equipment X' Pert pro PANalytical X-ray diffractometer with Cu-K α ($\lambda = 1.5406 \text{ \AA}$) radiation was used for powder XRD Studies. The Fourier transform infrared spectra (Shimadzu FTIR8400S) of the samples were recorded in the range $4000\text{--}500 \text{ cm}^{-1}$. The ac impedance measurements were carried out using computer controlled HIOKI 3532-50 LCR Hi TESTER over a frequency range of $42 \text{ Hz--}1 \text{ MHz}$ in the temperature range of $303\text{--}343 \text{ K}$ at every 10 K increment. All the measurements were obtained from the computer controlled software provided by the instrument. Since the solution cast methods do not produce samples of uniform thickness in the micrometer range. The thickness of the sample were measured at different regions using micrometer screw gauge. The difference between each measurement and the average value was not greater than 0.0010 cm . The dimensions of the samples involved thickness in the range of $0.0242\text{--}0.0257 \text{ cm}$. The average of all the measurement in thickness for the sample was taken for calculating conductivity so as to avoid error. The micrometer thick samples were sandwiched between two parallel stainless steel disc electrodes with surface contact area of 2.56 cm^2 in a conductivity cell and connected to LCR Meter. The data obtained from complex impedance were used to calculate dielectric parameters. Thermal studies were performed for the sample with highest conductivity using TA Instrument SDT Q600 V20.9 Build 20 at a heating rate of $10 \text{ }^\circ\text{C min}^{-1}$ from room temperature to $700 \text{ }^\circ\text{C}$ in nitrogen atmosphere. DSC analysis was carried out using TA Instrument DSC Q20 V24.10 Build 122 analyzer in the temperature range $0\text{--}175 \text{ }^\circ\text{C}$ at a heating rate of $10 \text{ }^\circ\text{C per minute}$ in nitrogen atmosphere. SEM analysis is carried out using VEGA3 TESCAN instrument to study the surface morphology of the samples.

3 Results and discussion

3.1 X-ray diffraction analysis

The powder X-ray diffraction measurements are carried out to study the crystalline nature and complexation

behaviour of CSPE sample T5 and compare it with individual polymer PMMA, SAN. It is evident from Fig. 1 that the CSPE sample T5 is amorphous in nature. Pure PMMA and SAN also exhibit amorphous nature. The presence of broad bands with no definite crystalline peaks shows amorphous behaviour [21]. The lithium triflate shows no characteristic peaks corresponding to its crystalline nature in the sample. This shows that the lithium triflate is completely dissociated and involved in interaction with the plasticizers and the polymer matrix [22]. The presence of the peaks characteristic of nano-filler anatase TiO₂ in sample T5 shows retention of crystalline nature of TiO₂ in the amorphous polymer blend matrix. There is increase in the 2 theta values for T5 Sample (2θ , 25.64) when compared with nano-filler TiO₂ (2θ , 24.92). This shift suggests that the nanofiller interact with polymeric host PMMA and the plasticizers EC and PC. This interaction weakens the interaction of polymeric host with the lithium salt. Also lithium ion and triflate ion of the lithium salt interacts with the filler leading to enhanced mobility while nano-filler TiO₂ retains its crystalline nature without undergoing degradation.

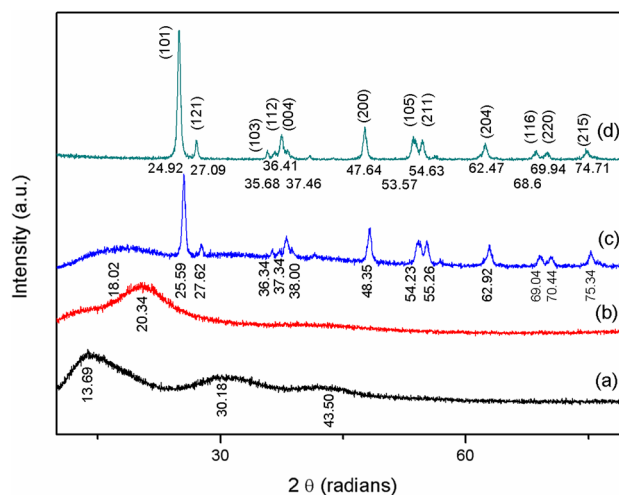


Fig. 1 XRD pattern of (a) pure PMMA, (b) pure SAN, (c) CSPE (T5) and anatase TiO₂

3.2 FTIR analysis

The FTIR spectroscopy studies are carried out on the samples with maximum conductivity (T5), minimum conductivity (T1) and compared with pure PMMA and pure SAN (Table 2; Fig. 2a, b). The symmetric and asymmetric bending mode vibrations of SO_3 group in both samples T1 and T5 (516 and 645 cm^{-1}) shows presence of free triflate (CF_3SO_3) anion [23]. The increase in frequency of stretching and bending vibrations of C–O–C in the samples T1 (1174 and 845 cm^{-1}) and T5 (1171 and 846 cm^{-1}) when compared with PMMA (1116 and 841 cm^{-1}) is due to the interaction of plasticizers EC and PC with lithium ion and also due to presence of CH_2 twisting and rocking vibrations. There is decrease in the vibrational stretching frequency of C–O and C–C–O bonds in samples T1 (1034 , 1258 cm^{-1}) and T5 (1034 , 1260 cm^{-1}) when compared to PMMA (1060 , 1386 cm^{-1}). This indicates that the carbonyl group of PMMA and the plasticizers EC and PC containing C–O bond interacts strongly with Li^+ ion [24]. There is decrease in vibrational stretching frequency of $-\text{OCH}_3$ in sample T5 (1487 cm^{-1}) compared to (1498 cm^{-1}) PMMA. Similarly, the vibrational deformation frequency of $-\text{OCH}_3$ group shows increase in value for T1 (1392 cm^{-1}) and T5 (1393 cm^{-1}) when compared to PMMA (1386 cm^{-1}). This indicates interaction of $-\text{OCH}_3$ group with lithium ion and

nano-filler TiO_2 . The increase in carbonyl stretching frequency for samples T1 and T5 (1730 cm^{-1}) when compared to PMMA (1710 cm^{-1}) is due to the presence and interaction of plasticizers EC and PC along with polymer blend containing PMMA with Lithium ion [25]. There is not much change in the C=C ring stretching and C–H ring bending vibrations in samples T1 and T5 compared to SAN. This indicates that the electron rich aromatic ring of the poly(styrene-co-acrylonitrile) does not interact with either Li ion or TiO_2 nano-filler. The presence of C–H alkyl and aromatic group are evidenced by corresponding SAN symmetric and asymmetric stretching vibrations around 2900 and 3000 cm^{-1} [26]. The nitrile stretching frequency in samples T1 and T5 (2236 cm^{-1}) is retained when compared with (2236 cm^{-1}) (SAN). The non-polar nature of the styrene present in the SAN prevents the $\text{C}\equiv\text{N}$ group of acrylonitrile from interaction with Li^+ ion as well as nano-filler TiO_2 .

3.3 AC impedance analysis

Figure 3 shows complex AC impedance spectra of the prepared composite polymer electrolytes with varying concentration of nano-filler TiO_2 (0, 5–9 wt%) respectively. There occurs a well defined semicircle in the high frequency region before a slanting spike in the low frequency region for sample T0 (without nano-filler TiO_2). The observed intercept

Table 2 Assignment of FT-IR vibrational peaks for PMMA, SAN, CSPE T1 and CSPE T5

	PMMA	SAN	T1	T5	Inference
			518	516.89	Symmetrical bending $\delta_s(\text{SO}_3)$
			645.14	645.14	Asymmetric bending $\delta_{as}(\text{SO}_3)$
		701	701	701	C–H ring out of plane bend
	750	759	760	759	CH_2 rocking
	841.87		845	846.69	C–O–C bending, CH_2 rocking
	988.45	967	988.45	988.45	CH_2 wagging
	1060.78	1070	1034.74	1034.74	C–O stretch, C–N stretch
	1116.71	1155	1174.57	1171.68	CH_2 twisting, C–O–C stretching
					C–H ring (in plane bend)
	1278.72		1258.47	1260.39	C–C–O stretching
	1386.72		1392	1393.47	O– CH_3 deformation
		1452.3	1450.37	1450.37	C=C ring stretching
	1498.59	1493.77	1493.77	1487.98	C–H ring bend, O– CH_3 stretch
	1710.74		1730.03	1729.06	C=O stretching
		2236.30	2237	2236	$\text{C}\equiv\text{N}$ stretching
	2339.49	2339.49	2348	2351	Over tone bands
	2359.74	2360.71	2377	2379	Over tone bands
		2918.1	2884.34	2888.93	Alkene C–H stretching
	2956.67		2946	2949.92	CH_3 stretching asymmetric
	3002		3000	2998.14	CH_3 stretching asymmetric
		3027.07	3026.1	3024.17	Aromatic C–H stretching

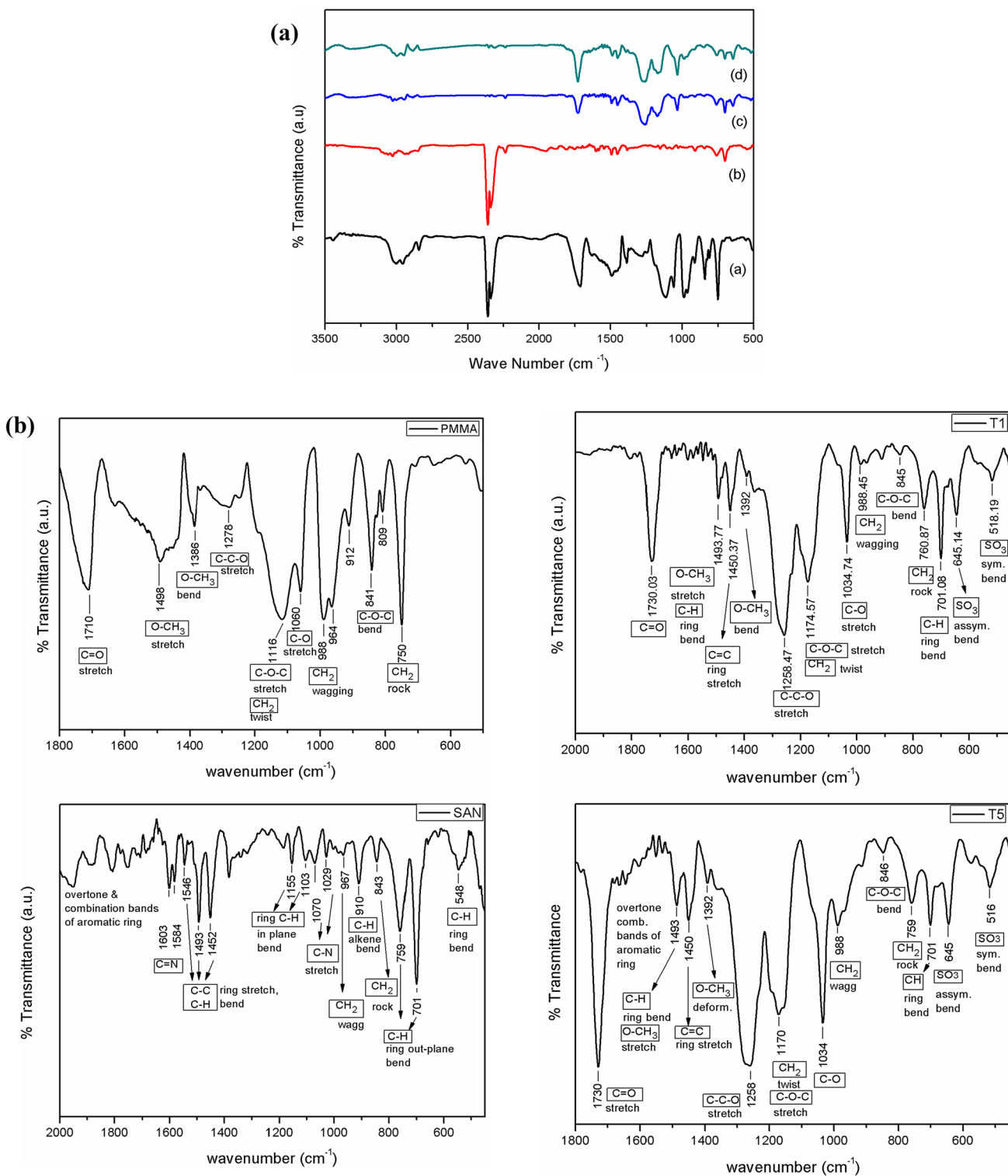


Fig. 2 a FT-IR spectra of (a) PMMA (b) SAN (c) CSPE (T1) and (d) CSPE (T5). b Assignment of peaks (~2000 to ~500 cm⁻¹ region) for PMMA, SAN, T1 and T5

of the plot in the high frequency semicircular region has been associated with the ionic conductivity process in the bulk of the composite polymer electrolytes. It is equivalent

to the parallel combination of bulk resistance and bulk capacitance. The low frequency spike has been attributed to the blocking double layer capacitance near the electrode/

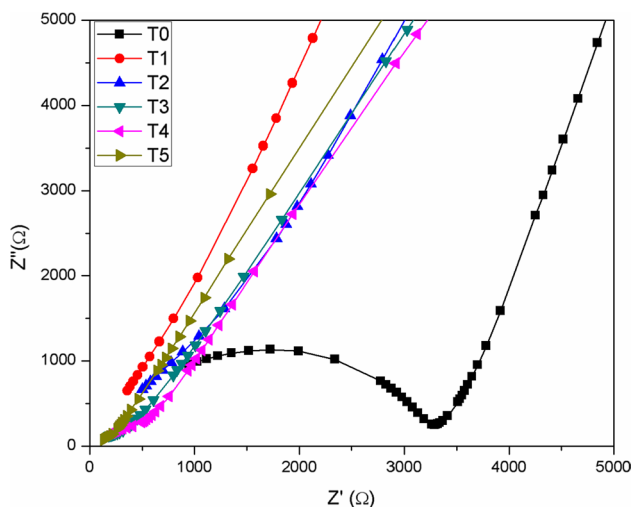


Fig. 3 Nyquist plot of CSPE's: PMMA-SAN-EC-PC-LiCF₃SO₃-xTiO₂; where x = 0 wt% (T0), 5 wt% (T1), 6 wt% (T2), 7 wt% (T3), 8 wt% (T4), 9 wt% (T5)

electrolyte interface due to ion migration [27]. Upon introduction of nano-filler TiO₂ into the polymer electrolyte containing lithium triflate salt, either absence or very negligible semicircle followed by slanting spike in the high frequency region is observed. The reduction or disappearance of semicircle in the high frequency region as the concentration of filler increases leads one to conclude that the majority current carriers and the conduction in electrolyte are contributed by ions and not electrons [28]. The attachment of lithium ions C=O and OCH₃ groups of PMMA are either broken or weakened by the introduction of nano-filler TiO₂. The oxygen atoms of the TiO₂ nanofiller compete with the PMMA polymer to attach with lithium ions. Lithium ions find enhanced number of sites for its transport. Thus ionic mobility of lithium ion is enhanced, leading to enhancement in ionic conductivity.

3.4 Concentration dependence conductivity

Ionic conductivity increased with increase in nano-filler TiO₂ concentration (Fig. 4). The maximum ionic conductivity of 1.05×10^{-4} S cm⁻¹ at room temperature and 1.95×10^{-4} S cm⁻¹ at 70 °C is obtained for sample T5 (9 wt% TiO₂) respectively. The increase in ionic conductivity is due to increase in number of free charge carriers (lithium ions) in the polymer matrix of the electrolyte [29, 30]. The enhancement of ionic conductivity is due to interaction of the acidic (Ti atoms) and basic (oxygen atoms) sites of the nano-filler TiO₂ with lithium and triflate ions of the lithium triflate salt, thereby reducing ion pairing between lithium and triflate ions leading to increase in the charge carrier density (involving lithium ions) [31]. However, further

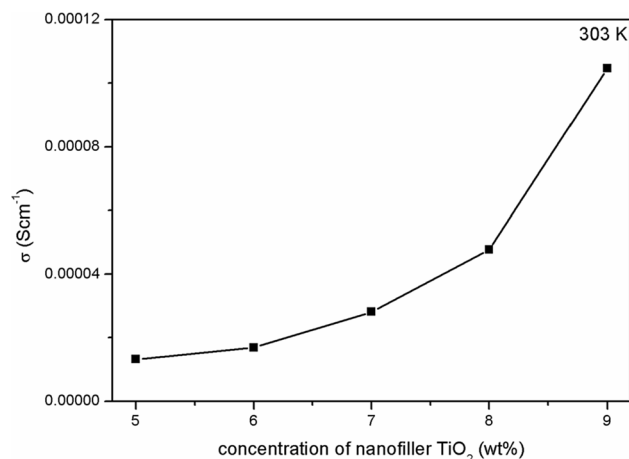


Fig. 4 Concentration of nano-filler TiO₂ (in wt%) vs ionic conductivity σ (S cm⁻¹) at room temperature for all the prepared CSPE samples

addition of nano-filler TiO₂ leads to agglomeration of the filler with lithium triflate salt that causes the sample to be rough, opaque and brittle (not suitable for analysis).

3.5 Temperature dependence conductivity

The values of ionic conductivity at different temperatures (303–343 K) as a function of nano-filler TiO₂ concentration in the prepared CSPE samples are listed in Table 3. The logarithmic plot of variation of conductivity as function of reciprocal of temperature for different concentration of nano-filler TiO₂ in the prepared CSPE samples is shown in Fig. 5. The linear variation of conductivity with respect to 1000/T for all prepared samples shows Arrhenius behavior. Thus, variation of conductivity (σ) with temperature (T) can be considered by the relation [32]:

$$\sigma = \sigma_0 \exp(-E_a/KT) \quad (2)$$

where σ_0 , E_a , and K refers to the pre-exponential factor, activation energy, and Boltzmann constant respectively. This observation can be explained by ion-hopping mechanism. As the temperature increases, the conductivity also increases. Therefore, the vibrational mode of polymer segments increases and gain sufficient energy to push against the hydrostatic pressure, imposed by its surrounding atoms and turns to the formation of voids [33]. At the same time, the polymer expands to produce the free volume [34], which leads to the interaction between the electron rich carbonyl oxygen as well as free electrons present in the methoxy group of the polymer backbones with Li⁺ ion. Thus, it promotes the charge carriers to the polymer matrix and enhances the ionic conductivity by way of segmental motion of the polymer chains [35]. The activation energy (E_a) in eV for Li⁺ ion transport is calculated from the slope of the Arrhenius plot and tabulated in Table 4. The regression

Table 3 Variation of ionic conductivity of CSPE samples with different concentration (wt%) of nano-filler anatase-TiO₂ at different temperatures

Sample	TiO ₂ wt%	σ (S cm ⁻¹)				
		303 K	313 K	323 K	333 K	343 K
T0	0	1.5 × 10 ⁻⁶	2.1 × 10 ⁻⁶	5.0 × 10 ⁻⁶	9.2 × 10 ⁻⁶	1.88 × 10 ⁻⁵
T1	5	1.32 × 10 ⁻⁵	1.86 × 10 ⁻⁵	2.65 × 10 ⁻⁵	3.77 × 10 ⁻⁵	5.39 × 10 ⁻⁵
T2	6	1.69 × 10 ⁻⁵	2.45 × 10 ⁻⁵	3.59 × 10 ⁻⁵	4.96 × 10 ⁻⁵	6.78 × 10 ⁻⁵
T3	7	2.17 × 10 ⁻⁵	3.16 × 10 ⁻⁵	4.78 × 10 ⁻⁵	6.78 × 10 ⁻⁵	9.97 × 10 ⁻⁵
T4	8	4.77 × 10 ⁻⁵	6.53 × 10 ⁻⁵	8.64 × 10 ⁻⁵	1.15 × 10 ⁻⁴	1.51 × 10 ⁻⁴
T5	9	1.05 × 10 ⁻⁴	1.26 × 10 ⁻⁴	1.46 × 10 ⁻⁴	1.69 × 10 ⁻⁴	1.95 × 10 ⁻⁴

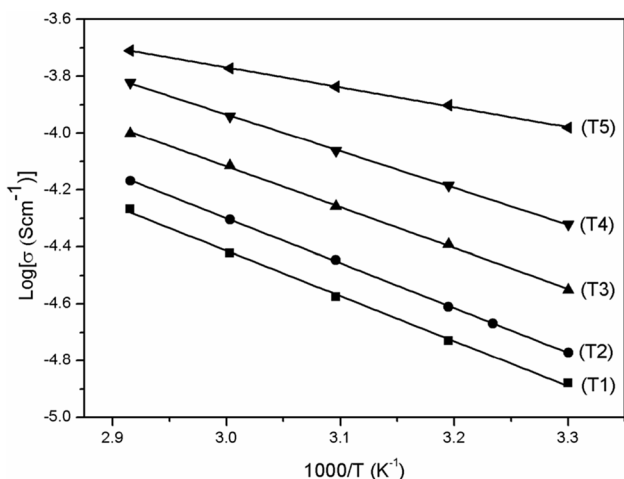


Fig. 5 Arrhenius Plot for different concentration of nano-TiO₂ filler in the prepared CSPE samples: T1=5 wt%, T2=6 wt%, T3=7 wt%, T4=8 wt%, T5=9 wt%

Table 4 Activation energy (E_a) with regression coefficient for different concentration of nano-filler TiO₂ in the prepared CSPE samples

S. no.	Sample	TiO ₂ wt%	Activation energy E _a (eV)	Regression value
1	T1	5	0.322	0.99
2	T2	6	0.315	1.00
3	T3	7	0.288	0.99
4	T4	8	0.259	1.00
5	T5	9	0.140	0.99

value is close to unity for all samples suggesting that all points lie on the straight line in Arrhenius plot.

Figure 6 shows that when concentration of nano-filler TiO₂ increases the activation energy (E_a) decreases, indicating Li⁺ ion requires less energy for migration. Hence, enhanced ionic conductivity is due to increased ionic mobility due to interaction with nanofiller TiO₂ and interaction of nanofiller TiO₂ with the polymer PMMA. Sample T5 containing 9 wt% of TiO₂ that exhibits highest

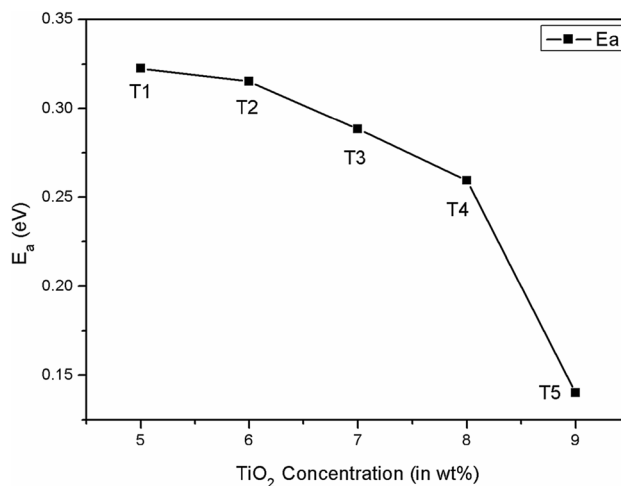


Fig. 6 Concentration of nano-filler TiO₂ (in wt%) vs. activation energy for all prepared CSPE samples

conductivity of 1.05 × 10⁻⁴ S cm⁻¹ at room temperature possess lowest activation energy (E_a = 0.14 eV).

3.6 Dielectric studies

Dielectric studies throw light on the relaxation behavior of electrolytes. Dielectric studies in the prepared CSPE samples help to identify their conductivity behavior. Real and imaginary parts of complex permittivity (ε*) also known as dielectric constant (ε') and dielectric loss (ε'') are derived from measured impedance data using the following relation [36]:

$$\epsilon^* = \epsilon'(\omega) - i\epsilon''(\omega) \tag{2}$$

Figures 7 and 8 shows the frequency-dependent plot of ε' and ε'' parts of dielectric permittivity curves. From the graph, it is observed that both ε' and ε'' increase toward low frequency and gradually slowly approaching zero at high frequency. At the very low frequencies (f < 1/τ, where τ is the relaxation time), dipoles follow the electric field. As the frequency increases, dipoles begin to lag behind the field and slightly decrease. When the frequency reaches the characteristic frequency (f = 1/τ), the dielectric constant

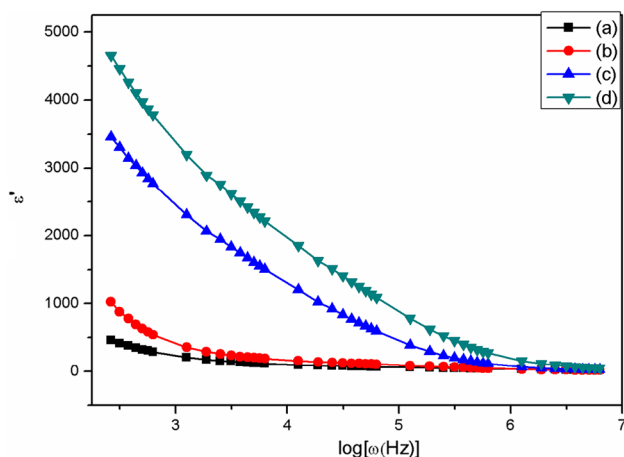


Fig. 7 Variation of real part of dielectric constant (ϵ') as a function of angular frequency (ω) for different concentration of nano-TiO₂ filler in the prepared CSPE samples: (a) 5 wt%, (b) 6 wt%, (c) 7 wt%, (d) 9 wt%

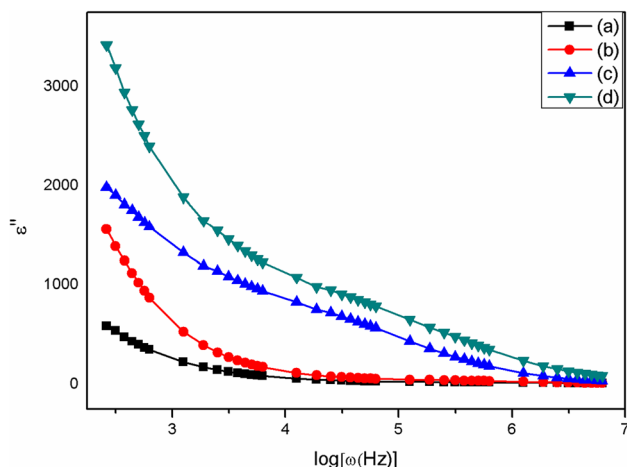


Fig. 8 Variation of imaginary part of dielectric constant (ϵ'') as a function of angular frequency (ω) for different concentration of nano-TiO₂ filler in the prepared CSPE samples: (a) 5 wt%, (b) 6 wt%, (c) 7 wt%, (d) 9 wt%

drops (relaxation process). At the very high frequencies ($f > 1/\tau$), dipoles can no longer follow the field and $\epsilon' \approx \epsilon'_{\infty}$. Hence dielectric constant ϵ' and dielectric loss ϵ'' gradually approach zero. Higher values of dielectric constant at the low frequencies can be explained as due to the formation and accumulation of the charges at the grain boundaries and at the interfaces between the electrolyte and the electrode (known as space charge polarization). This is well known as the non-Debye type of behavior, where the ion diffusion explains the space charge regions with respect to the frequency [26].

As the concentration of nano-filler TiO₂ increases, the dielectric constant increases. The highest value for both ϵ'

and ϵ'' is observed at 9 wt% salt. The increase of dielectric constant with respect to filler content is due to the enhanced charge carrier density in the space charge accumulation region, which caused the enhancement of equivalent capacitance [37]. This means that the sample T5 containing 9 wt% of nano-filler TiO₂ has the maximum number of charge carriers stored. Since the graph does not show any relaxation peaks, this indicates that the increase in conductivity value is due to increase in free charge carriers and their retention [38]. The same trend for dielectric loss (ϵ'') is observed as for dielectric constant (ϵ'). No appreciable relaxation peaks were observed. This indicates that the increase in the concentration of nano-filler leads to increase in the degree of salt dissociation and further dissociation of ion aggregates, leading to increase in the number of free ion and their mobility that in turn increases the conductivity of the sample [39].

3.7 Loss tangent spectra

The dielectric relaxation parameter of the prepared CSPE samples can be obtained from study of dielectric loss tangent ($\tan \delta$) as a function of angular frequency (ω). The dielectric loss tangent ($\tan \delta$) is given by the relation:

$$\tan \delta = \epsilon'' / \epsilon' \quad (3)$$

It is observed that the dielectric loss tangent increases with increase in angular frequency and reaches a peak value. Further increase in angular frequency leads to decrease in the dielectric loss tangent values. The dielectric relaxation time (τ) can be obtained from the angular frequency (ω) corresponding to dielectric loss tangent ($\tan \delta$) peak as follows:

$$\omega\tau = 1 \quad (4)$$

Thus, dielectric relaxation time (τ) = $1/\omega$.

The dielectric relaxation time (τ) for different concentration of nano-filler TiO₂ in the prepared CSPE samples are calculated from the dielectric loss tangent spectra depicted in Fig. 9. The obtained angular frequency (ω) and dielectric relaxation time (τ) are tabulated in Table 5. From the Fig. 9, it is observed that the dielectric loss tangent peak shifts towards higher angular frequency with increase in the concentration of the nano-filler TiO₂. This indicates that concentration of charge carrier lithium ions increases with increase in filler content. Also the shift towards higher frequency leads to shorter relaxation time (Table 5). The sample T5 possess shortest relaxation time (1.49×10^{-7} s) and highest conductivity (1.05×10^{-4} S cm⁻¹) among the prepared CSPE samples. Thus the increase in the concentration of nano-filler TiO₂ leads to increase in the ionic mobility and number density of charge carrier lithium ions. Relatively fast segmental motion of the polymer chain coupled with increased number of charge carriers lithium ions leads to enhanced transport properties of the polymer electrolyte

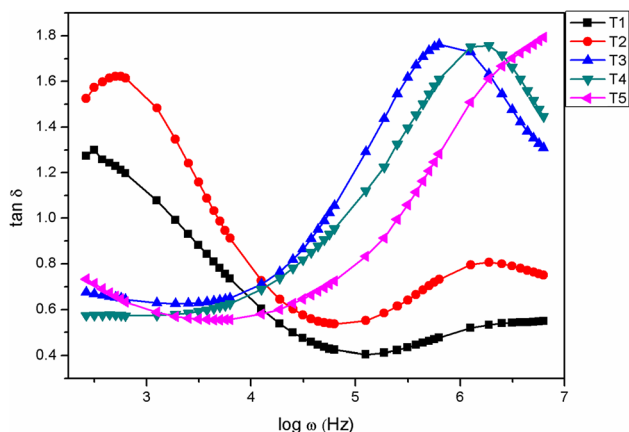


Fig. 9 Variation of $\tan \delta$ as a function of angular frequency (ω) for different concentration of nano-TiO₂ filler in the prepared CSPE samples: T1 = 5 wt%, T2 = 6 wt%, T3 = 7 wt%, T4 = 8 wt%, T5 = 9 wt%

Table 5 Relaxation time (τ) for the prepared CSPE samples at room temperature

S. no.	Sample	TiO ₂ wt%	Angular frequency (ω_{max})	Relaxation time (τ)
1	T1	5	3.14×10^2	3.18×10^{-3}
2	T2	6	5.64×10^2	1.77×10^{-3}
3	T3	7	6.35×10^5	1.57×10^{-6}
4	T4	8	1.24×10^6	8.07×10^{-7}
5	T5	9	6.71×10^6	1.49×10^{-7}

system, thus relaxation time decreases with increase in conductivity [40].

3.8 Thermogravimetric analysis

Figure 10 represents TG/DTG thermogram of highest conducting plasticized composite solid polymer electrolyte sample T5. The TG curve shows gradual weight loss of 9% up to 169 °C. This initial weight loss is due to the presence of solvent and little moisture while loading the sample [41]. The film is found to be stable from 169 to 333 °C with a weight loss of 6%, after which the sample undergoes drastic weight loss of 54% at 439 °C. This may be due to degradation of the polymer electrolyte leading to melting and evaporation of its components [13]. Subsequent weight loss around 10% may be due to the melting and evaporation of lithium triflate salt components, leaving behind carbon, filler and lithium residue amounting to 20%. From the above analysis, the prepared highest conducting composite solid polymer electrolyte sample T5 is found to be stable up to 333 °C after complete removal of residual solvent, moisture and its impurities.

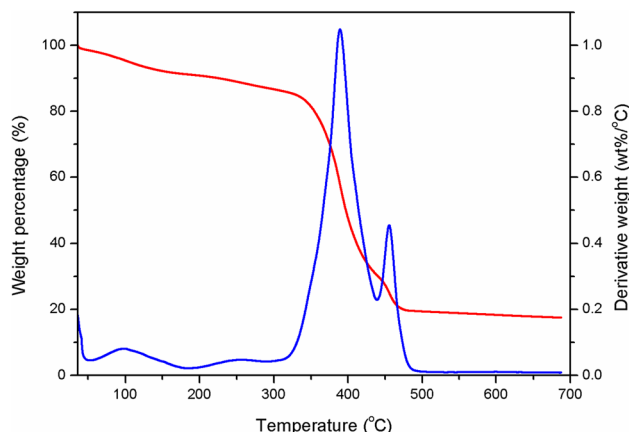


Fig. 10 TG/DTG curve of CSPE (T5)

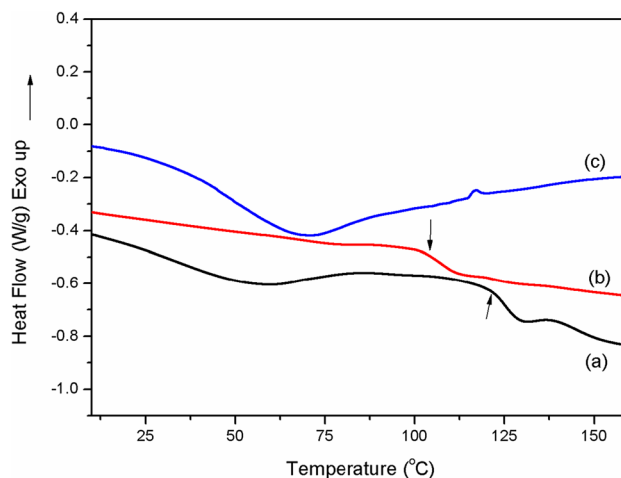


Fig. 11 DSC curves of (a) pure PMMA, (b) pure SAN and (c) CSPE (T5)

3.9 DSC analysis

From Fig. 11, DSC Analysis provides the T_g values of pure PMMA and SAN at 120 and 100 °C respectively. The incorporation of plasticizers EC and PC into the above system involving PMMA, SAN and Lithium triflate leads to complete miscibility and thus exhibits only one T_g value at 107.3 °C [42]. This shows that the plasticizers help to solvate the lithium ions and make it miscible with polymer blend system by providing more amorphous rich phase [43]. In the presence of nanofiller TiO₂ (9 wt%) the CSPE exhibits no glass transition temperature corresponding to atactic component of PMMA. This shows that incorporating crystalline nano-filler TiO₂ does not influence upon amorphous nature of the polymer electrolyte system and the polymer blends do not undergo crystallization. Therefore, it is suggested that the incorporation of nano-filler TiO₂ does interact strongly

with polymer PMMA while SAN is inert. The nano-filler interacts with the lithium triflate salt preventing ion aggregation and enhancing further dissociation of ion aggregates leading to increased charge carrier density and ionic mobility [44]. Therefore, increase in the concentration of nano-filler leads to enhancement in ionic conductivity.

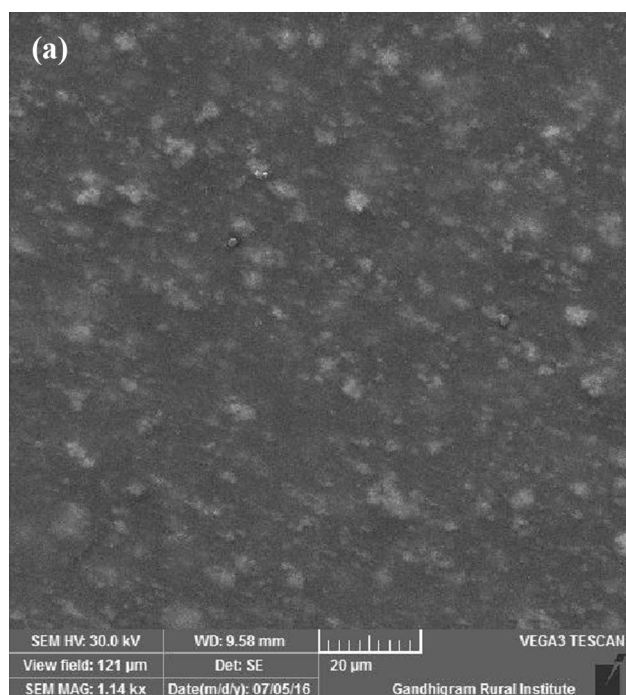
3.10 SEM morphology

The surface morphology of the CSPE with highest (T5) and lowest conductivity (T1) are depicted in the Fig. 12 through SEM micrographs. SEM Analysis throws light on the surface morphology, formation of grains and gives information on the pores and irregularities present on the polymer electrolyte surface. Thus surface morphology influences ionic conductivity as well as stability of the polymer electrolyte films.

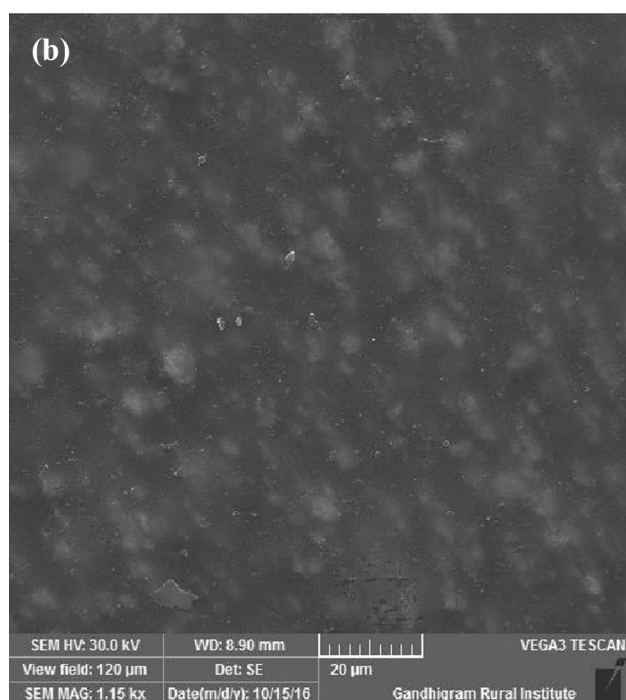
The CSPE sample T1 (5 wt% TiO_2) shows rough surface but irregular dispersion of the filler on the polymer blend matrix (Fig. 12a). The filler particles are not embedded into the system. The CSPE sample T5 (9 wt% TiO_2) shows surface morphology in which the presence of nano-filler TiO_2 and lithium triflate salt with the polymer electrolyte surface does not lead to heterogeneity of the polymer blend (Fig. 12b) [41]. The amorphous nature is retained thus enhancing ionic mobility and hence ionic conductivity.

4 Conclusion

PMMA and SAN based composite solid polymer electrolyte involving plasticizers EC and PC with lithium triflate as salt and varying concentration of nano-filler TiO_2 is prepared by solution casting technique using THF as solvent. The absence of XRD peaks characteristic of lithium triflate salt in CSPE with highest conductivity (T5) reveal that the Li^+ ion is solvated by plasticizers and involved in interactions with the polymer blend system leading to more amorphous nature of the CSPE. The retention of crystalline nature of TiO_2 shows no degradation or transformation of the nano-filler in the composite solid polymer electrolyte system. The interaction of nano-filler with polymer host is confirmed by shift in the 2 theta position of peaks when compared with XRD peaks of nano-filler TiO_2 . FT-IR studies reveal interaction of Lithium ion with both $\text{C}=\text{O}$ and OCH_3 group of the PMMA. The $\text{C}\equiv\text{N}$ group of SAN does not interact with Lithium ion as more non-polar nature of styrene prevents nitrile group of acrylonitrile from interaction with Lithium ion. The ionic conductivity of the prepared CSPE samples increase with increase in the concentration of nano-filler TiO_2 . The temperature dependence of ionic conductivity follows Arrhenius relation. The dielectric studies reveal increase in the dielectric constant (ϵ') and dielectric loss (ϵ'') with increase in the concentration of nano-filler TiO_2 .



CSPE (T1)



CSPE (T5)

Fig. 12 Scanning electron microscope image of (a) CSPE T1 and (b) CSPE T5

The absence of relaxation peaks in the dielectric constant and dielectric loss spectra suggest that the prepared CSPE samples are ionic conductors. The study of dielectric loss tangent spectra reveals shift towards higher frequency leading to shorter relaxation time τ , with increase in concentration of nano-filler TiO_2 . The CSPE sample T5 possess shortest relaxation time (1.49×10^{-7} s), lowest activation energy ($E_a = 0.14$ eV) and highest conductivity (1.05×10^{-4} S cm^{-1}) at room temperature among the prepared CSPE samples. Thus the increase in the concentration of nano-filler TiO_2 leads to increase in the ionic mobility and charge carrier density that combined with polymer chain segmental motion of amorphous polymer blend involving PMMA and SAN in a plasticized (EC and PC) environment leads to enhanced conductivity of the prepared CSPE samples. TG/DTG studies reveal thermal stability of highest conducting sample T5 up to 333 °C after complete removal of residual solvent, moisture and its impurities. DSC studies reveal absence of glass transition temperature (T_g) corresponding to atactic component of PMMA for CSPE T5 when compared with individual polymers PMMA (120 °C), SAN (100 °C) and their blend with Lithium triflate salt PSL3 (107 °C). This shows that the incorporation of nano-filler TiO_2 leads to increased amorphous nature of the polymer electrolyte system when compared with either of the individual polymer PMMA and SAN. The nano-filler interacts with the lithium triflate salt preventing ion aggregation and enhancing further dissociation of ion aggregates leading to increased charge carrier density and ionic mobility. Therefore, increase in the concentration of nano-filler leads to enhancement of ionic conductivity. Morphological studies using SEM analysis reveals the presence of lithium salt and filler TiO_2 on polymer host does not lead to heterogenous polymer blend thus retaining its amorphous nature.

References

1. A.M. Stephan, *Eur. Polym. J.* **42**, 21–42 (2006)
2. G.B. Appetecchi, B. Scrosati, *Electrochim. Acta* **39**, 2187–2194 (1994)
3. E. Quartarone, P. Mustarelli, *Chem. Soc. Rev.* **40**, 2525–2540 (2011)
4. S. Ahmad, S. Ahmad, S.A. Agnihotry, *Ionics* **9**, 439–449 (2003)
5. J. Adebahr, N. Byrne, M. Forsyth, D.R. MacFarlane, P. Jacobsson, *Electrochim. Acta* **48**, 2099–2103 (2003)
6. H.M. Xiong, J.S. Chen, D.M. Li, *J. Mater. Chem.* **13**, 1994–1998 (2003)
7. F. Croce, S. Sacchetti, B. Scrosati, *J. Power Sources* **161**, 560–564 (2006)
8. J.E. Weston, B.C.H. Steele, *Solid State Ionics* **71**, 75–79 (1982)
9. S.K. Hyung, S.K. Kyong, C. Won-II, W.C. Byung, W.R. Hee, *J. Power Sources* **124**, 221–224 (2003)
10. J. Srun, W.K. Dae, D.L. Sang, C. Minserk, Q.N. Dinh, W.C. Byung, S.K. Hoon, *Bull. Korean Chem. Soc.* **30**, 2355–2361 (2009)
11. G.N. Kumaraswamy, C. Ranganathaiah, M.V. Deepa Urs, H.B. Ravikumar, *Eur. Polym. J.* **42**, 2655–2666 (2006)
12. D. Miao, G. Jianhua, Z. Qiang, *Polymer* **45**, 6725–6730 (2004)
13. S. Ramesh, K.C. Wong, *Ionics* **15**, 249–254 (2009)
14. L. Othman, K.W. Chew, Z. Osman, *Ionics* **13**, 337–342 (2007)
15. S. Ramesh, L.C. Wen, *Ionics* **16**, 255–262 (2010)
16. H. Li, M. Zuo, T. Liu, Q. Chen, J. Zhang, Q. Zheng, *RSC Adv.* **6**, 10099–10113 (2016)
17. C. Lin, M. Zuo, H. Li, T. Liu, Q. Zheng, *Chin. J. Polym. Sci.* **33**(8), 1162–1175 (2015)
18. A. Sarvi, U. Sundararaj, *Polym. Compos.* **37**(5), 1523–1530 (2016)
19. M. Lee, H. Jeon, B.H. Min, J.H. Kim, *J. Appl. Polym. Sci.* **121**(2), 743–749 (2011)
20. I. Nicotera, L. Coppola, C. Oliviero, M. Castriota, E. Cazzanelli, *Solid State Ionics* **177**, 581–588 (2006)
21. S. Rajendran, O. Mahendran, T. Mahalingam, *Eur. Polym. J.* **38**, 49–55 (2002)
22. M.S. Su'ait, A. Ahmad, H. Hamzah, M.Y.A. Rahman, *Electrochim. Acta* **57**, 123–131 (2011)
23. R. Kumar, J.P. Sharma, S.S. Sekhon, *Eur. Polym. J.* **41**, 2718–2724 (2005)
24. A.M.M. Ali, M.Z.A. Yahya, H. Bahron, R.H.Y. Subban, M.K. Harun, I. Atan, *Mater. Lett.* **61**, 2026–2029 (2007)
25. K.W. Chew, K.W. Tan, *Int. J. Electrochem. Sci.* **6**, 5792–5801 (2011)
26. L. Tian Khoon, N. Ataollahi, N.H. Hassan, A. Ahmad, *J. Solid State Electrochem.* **20**, 203–213 (2016)
27. A.R. Polu, H.W. Rhee, D.K. Kim, *J. Mater. Sci. Mater. Electron.* **11**, 8548–8554 (2015)
28. M.M.E. Jacob, S.R.S. Prabaharan, S. Radhakrishna, *Solid State Ionics* **104**, 267–274 (1997)
29. T.K. Lee, A. Ahmad, H.M. Dahlan, M.Y.A. Rahman, *J. Appl. Polym. Sci.* **124**, 2227–2233 (2012)
30. T.K. Lee, S. Afiqah, A. Ahmad, H.M. Dahlan, M.Y.A. Rahman, *J. Solid State Electrochem.* **16**, 2251–2260 (2012)
31. S. Rajendran, O. Mahendran, K. Krishnaveni, *J. New Mat. Electrochem. Syst.* **6**, 25–28 (2003)
32. A.S. Samsudin, M.B.N. Isa, *J. App. Sci.* **12**, 174–179 (2012)
33. S. Rajendran, M. Sivakumar, R. Subadevi, *Mater. Lett.* **58**, 641–649 (2004)
34. J.D. Jeon, S.Y. Kwak, B.W. Cho, *J. Electrochem. Soc.* **152**, 1583–1589 (2005)
35. V. Aravindan, P. Vickraman, *Solid State Sci.* **9**, 1069–1073 (2007)
36. M.V. Leena Chandra, S. Karthickeyan, S. Selvasekarapandian, M. Premalatha, S. Monisha, *J. Polym. Eng.* **37**, 617–631 (2016)
37. S. Ramesh, P.L. Ong, *Polym. Chem.* **1**, 702–707 (2010)
38. S.K. Tripathi, A. Gupta, M. Kumari, *Bull. Mater. Sci.* **35**, 969–975 (2012)
39. S. Shastry, K.J. Rao, *Solid State Ionics* **44**, 187–198 (1991)
40. K. Ramly, M.I.N. Isa, A.S.A. Khiar, *Mater. Res. Innov.* **15**, S82 (2011)
41. X. Helan Flora, M. Ulaganathan, R.S. Babu, S. Rajendran, *Ionics* **18**, 731–736 (2012)
42. J.M. Song, H.R. Kang, S.W. Kim, W.M. Lee, H.T. Kim, *Electrochim. Acta* **48**, 1339–1346 (2003)
43. R. Prasanth, V. Aravindan, M. Srinivasan, *J. Power Sources* **202**, 299–307 (2012)
44. M.A.K.L. P.A.R.D. Jayathilaka, I. Dissanayake, B.E. Albbinsson, Mellander, *Electrochim. Acta* **47**, 3257–3268 (2002)